CORROSION SCIENCE AND TECHNOLOGY, Vol.25, No.2(2026), pp.63~81 pISSN 1598-6462 / eISSN 2288-6524
[Research Paper] DOI: https://doi.org/10.14773/cst.2026.25.2.63

Multifunctional Corrosion Inhibition of Mild Steel in Hydrochloric Acid by 6-(N-morpholino)-2-carboxypyrazine: Surface Adsorption, Electrochemical, Thermodynamic, and Quantum Insights

Wael H. Alsadi[1] and Ahmed A. Alamiery[2,†]

[1]*Department of Chemistry, Faculity of Science, Taibah University, PO. BOX 30002, Al-Madinah Al-Munawarah, Medina, Saudi Arabia*
[2]*Al-Ayen Scientific Research Center, Al-Ayen Iraqi University, AUIQ, An Nasiriyah, P.O. Box: 64004, Thi Qar, Iraq*
(Received July 07, 2025; Revised August 06, 2025; Accepted August 20, 2025)

The effectiveness of 6-(N-morpholino)-2-carboxypyrazine (MCP) as a corrosion inhibitor for mild steel in 1 M hydrochloric acid was systematically assessed using weight loss measurements, electrochemical techniques, and quantum chemical calculations. Various concentrations of the inhibitor (0.0–0.5 mM) and immersion times (1–48 hours) were tested at 303 K, along with temperature variations (303–333 K) to evaluate thermodynamic parameters. The inhibition efficiency increased with concentration, peaking at 81.9% from potentiodynamic polarization and 83.8% from weight loss at 0.5 mM, with moderate enhancement observed at higher temperatures, indicating a chemisorptive interaction. The adsorption behavior followed the Langmuir isotherm, suggesting the formation of a monolayer on the metal surface. Potentiodynamic polarization studies identified MCP as a mixed-type inhibitor, effectively slowing both anodic metal dissolution and cathodic hydrogen evolution. Density functional theory (DFT) computations corroborated these findings by indicating a low HOMO-LUMO energy gap and favorable charge distribution, which align with strong surface adsorption. Together, these experimental and theoretical results position MCP as a thermally stable, electronically active, and surface-affinitive corrosion inhibitor, presenting promising potential for the development of protective coatings for steel structures in acidic environments.

Keywords: *Morpholino, Corrosion inhibitor, Potentiodynamic, Langmuir, DFT*

1. Introduction

Corrosion, the gradual degradation of materials usually metals due to chemical reactions with their environment, is a persistent industrial and economic problem worldwide. Among various types of corrosion, acid-induced corrosion of mild steel is particularly critical due to its extensive use in industries such as petroleum refining, chemical processing, power generation, and infrastructure construction [1-3]. Hydrochloric acid (HCl), commonly used in industrial cleaning and pickling processes, aggressively attacks mild steel, leading to material loss, equipment failure, and significant economic burden. To combat such damage, the use of corrosion inhibitors has emerged as an effective and economical strategy [4]. Corrosion inhibitors are substances that, when added in small concentrations to a corrosive medium, significantly reduce the rate of metal dissolution. Organic inhibitors are especially appealing due to their wide structural variety and ability to be tailored for performance. Typically, these inhibitors contain heteroatoms such as nitrogen, sulfur, and oxygen that facilitate adsorption onto the metal surface, forming a protective barrier that impedes corrosive species [5,6]. In recent years, heterocyclic organic compounds have shown immense promise as corrosion inhibitors. Their effectiveness is mainly attributed to their ability to adsorb onto metal surfaces through π-electrons and lone pairs present on heteroatoms, forming a stable chemisorbed layer that blocks aggressive ions [7-9]. A substantial body of literature supports the efficacy of morpholine and its derivatives as corrosion inhibitors, particularly in aggressive acidic environments such as hydrochloric acid [10-13]. These nitrogen- and oxygen-containing heterocyclic compounds possess unique structural features that enable efficient adsorption onto metal

[†]Corresponding author: dr.ahmed1975@gmail.com

surfaces, leading to protective film formation and inhibition of electrochemical reactions involved in corrosion [14-16]. Quantum chemical parameters including HOMO and LUMO energies, dipole moments, and electron density distributions support the theoretical basis for their strong reactivity and efficient surface binding. These combined attributes render morpholine derivatives highly adaptable and tunable for corrosion inhibition in diverse industrial contexts. The present study on MCP is a continuation and enhancement of this research lineage, demonstrating high inhibition efficiency, robust adsorption characteristics, and thermodynamic favorability. Through an integrated approach that includes weight loss experiments, electrochemical measurements, adsorption modeling, and density functional theory (DFT) calculations, this inhibitor emerges as a highly promising candidate for corrosion mitigation applications, particularly in aggressive acidic environments like hydrochloric acid. The primary aim of this study is to evaluate the effectiveness of *MCP* as a corrosion inhibitor for mild steel in 1 M hydrochloric acid solution. This work will contribute to the ongoing development of eco-friendly and cost-effective corrosion inhibitors.

To the best of our knowledge, this study presents the first report on the corrosion inhibition behavior of MCP on mild steel in HCl. While both morpholine and pyrazine derivatives have been individually studied as organic inhibitors, MCP uniquely integrates these two moieties into a single hybrid molecule, offering multiple adsorption-active centers such as nitrogen, oxygen, and carboxyl functional groups. This structural synergy enhances surface affinity, enabling both π–d orbital interactions and coordinate bonding with iron atoms. Furthermore, the comprehensive approach used combining weight loss, electrochemical, thermodynamic, and quantum chemical analyses provides a holistic understanding of MCP's inhibition mechanism. The dual-functional nature and the multi-technique validation of MCP establish its novelty and potential as an advanced, multifunctional corrosion inhibitor for industrial applications. The combination of experimental and theoretical tools will not only establish MCP (Fig. 1) as a viable inhibitor but also deepen the understanding of structure-property-performance relationships in morpholine-based inhibitors. The findings are expected to support industrial applications requiring corrosion control in acidic environments and guide the rational design of next-generation inhibitors.

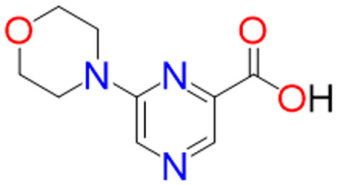

Fig. 1. The chemical structure of *MCP*

2. Materials and Methodologies

2.1 Reagents and Preparation of Mild Steel Samples

All chemicals utilized in this study were of analytical purity and sourced from Sigma-Aldrich (Malaysia). The compound *MCP* served as the corrosion inhibitor and was used as received, without additional purification steps. Its purity was verified via thin-layer chromatography (TLC) on silica gel G plates, ensuring the absence of secondary components or degradation products. Mild steel (MS) specimens, provided by Gamry Instruments Inc., were employed as the metallic substrate throughout all experiments. The exposed surface area for each metal coupon was fixed at 4.5 cm^2. The chemical composition of the mild steel (in wt%) was as follows: Fe (99.21%), C (0.21%), Si (0.38%), P (0.09%), S (0.05%), Mn (0.05%), and Al (0.01%). Prior to experimentation, all samples underwent a standardized surface treatment procedure in compliance with ASTM G1-03 guidelines [17,18]. This involved sequential mechanical polishing using silicon carbide abrasive papers with increasing grit sizes (ranging from 400 to 1200), rinsing with distilled water, ultrasonic degreasing in acetone, and finally air-drying under ambient conditions.

2.2 Weight Loss (Gravimetric) Investigations

Gravimetric analysis was adopted to quantify corrosion rates and inhibition efficiencies in the presence and absence of the inhibitor compound. Pre-weighed mild steel coupons with an exposed surface of 1 cm^2 were fully immersed in 500 mL of 1.0 M hydrochloric acid solutions containing varying concentrations of *MCP* (0.0, 0.1, 0.2, 0.3, 0.4, and 0.5 mM). The experiments were conducted in a thermostatically controlled bath at four different

temperatures: 303 K, 313 K, 323 K, and 333 K. Each sample was exposed to the test solution for immersion durations of 1, 5, 10, 24, and 48 hours depending on the experimental objective. Upon retrieval, the specimens were rinsed thoroughly in deionized water and ethanol, followed by ultrasonic cleaning to remove residual surface products. The cleaned samples were dried under vacuum and reweighed using an analytical balance with ±0.0001 g sensitivity [19]. All weight loss measurements were performed in triplicate, and the reported results represent average values, with standard deviations included in the graphical and tabulated data to ensure statistical reliability and reproducibility. The corrosion rate (C_R), inhibition efficiency (IE%), and surface coverage (θ) were determined using the following formulas (1)-(3):

$$C_R = \frac{W}{at} \tag{1}$$

$$IE\% = \left[1 - \frac{C_{R(i)}}{C_{R(o)}}\right] \times 100 \tag{2}$$

$$\theta = 1 - \frac{C_{R(i)}}{C_{R(o)}} \tag{3}$$

where W is the weight loss in grams, a is the exposed surface area of the steel sample in cm², and t is the immersion time in hours, $C_{R(o)}$ is the corrosion rate without the inhibitor (control) and $C_{R(i)}$ is the corrosion rate in the presence of inhibitor.

Fig. 2 shows a simplified representation of the setup, in which a suspended steel sample is held in place within the acidic solution inside a glass beaker.

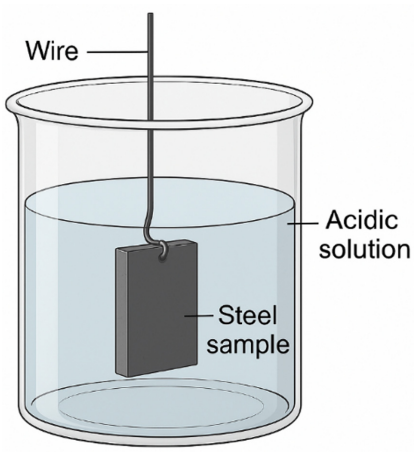

Fig. 2. Experimental Setup for Weight Loss Corrosion Test

2.3 Electrochemical Analysis

To complement the weight loss results, electrochemical assessments were performed in aerated, unstirred 1.0 M HCl medium. The electrochemical measurements were carried out at room temperature using a high-precision Gamry Interface REF600 electrochemical workstation. A standard three-electrode system was employed: mild steel served as the working electrode (WE), a saturated calomel electrode (SCE) acted as the reference electrode (RE), and a platinum wire was used as the counter electrode (CE). Prior to polarization measurements, each working electrode was stabilized in the test solution for 30 minutes to achieve a steady-state open circuit potential (OCP). Potentiodynamic polarization curves were obtained by scanning the electrode potential from −200 mV to +200 mV relative to the OCP at a fixed rate of 0.5 mV/s [20].

The Tafel extrapolation method was used to extract electrochemical parameters such as corrosion potential (E_{corr}), corrosion current density (I_{corr}), and anodic and cathodic Tafel slopes (βa and βc) [21]. All electrochemical measurements were conducted in triplicate, and the data presented reflect average values. Standard deviations and error bars are included where applicable to highlight the reproducibility and reliability of the results. The inhibition efficiency from polarization measurements was computed using the relation (4):

$$IE\% = \left(1 - \frac{I_{corr}^{inh}}{I_{corr}^{blank}}\right) \tag{4}$$

Where I_{corr}^{inh} and I_{corr}^{blank} denote the corrosion current densities in the presence and absence of the inhibitor, respectively. All electrochemical tests were repeated five times to ensure statistical consistency and reproducibility.

2.4 Quantum Chemical Calculations (DFT Method)

To provide molecular-level insight into the adsorption behavior and reactivity of the inhibitor, density functional theory (DFT) calculations were conducted. The computations were executed using a custom-built DFT software employing the Becke-3-Lee-Yang-Parr (B3LYP) functional combined with the 6-31G(d) basis set [22,23]. The

optimized molecular geometry of *MCP* was obtained through energy minimization. Key quantum chemical descriptors such as highest occupied molecular orbital energy (E_{HOMO}), lowest unoccupied molecular orbital energy (E_{LUMO}), ionization potential (I), electron affinity (A), chemical hardness (η), electronegativity (χ), softness (σ), and the fraction of electron transfer (ΔN) were calculated using the following expressions (5)-(10):

Ionization potential (I): $I = -E_{HOMO}$ (5)

Electron affinity (A): $A = -E_{LUMO}$ (6)

Electronegativity (χ): $\chi = \frac{I + A}{2}$ (7)

Chemical hardness (η): $\eta = \frac{I - A}{2}$ (8)

Chemical softness (σ): $\sigma = \eta^{-1}$ (9)

$$\Delta N = \frac{7 - \chi_{inh}}{2\eta_{inh}} \quad (10)$$

In this analysis, the electronegativity and hardness values for iron were taken as 7.0 eV and 0.0 eV respectively, as standard reference values.

These descriptors provided critical insights into the inhibitor's electron-donating and accepting tendencies, which relate directly to its interaction with the mild steel surface, supporting the experimental data obtained through gravimetric and electrochemical techniques.

3. Results and Discussion

3.1 Effect of Inhibitor Concentration on Corrosion Behavior at 303 K (Weight Loss Method)

The influence of MCP concentration on the corrosion rate (C_R) and inhibition efficiency (IE%) of mild steel in 1.0 M HCl was studied using weight loss measurements after a fixed immersion time of 5 hours at 303 K. The obtained results are graphically illustrated in Fig. 3.

The corrosion rate decreased markedly with the addition of the inhibitor, demonstrating its effective performance in mitigating acid-induced metal dissolution. In the absence of the inhibitor (0.0 mM), the corrosion rate was recorded at 3.20 mg·cm^{-2}·h^{-1}. Upon increasing the concentration to 0.1 mM, the C_R dropped sharply to

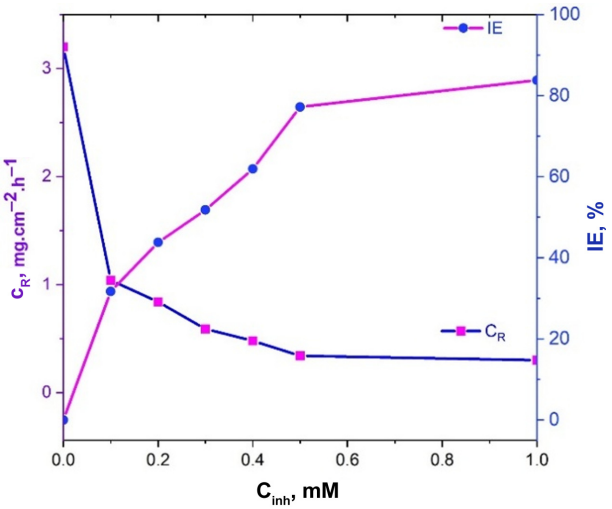

Fig. 3. Effect of MCP Concentration on C_R and IE% of Mild Steel in 1 M HCl

1.04 mg·cm^{-2}·h^{-1}, translating to an inhibition efficiency of 31.7%**.** This immediate decline indicates that even at low concentrations, MCP begins to adsorb onto the steel surface, reducing active dissolution sites. Further increases in concentration to 0.2 and 0.3 mM led to additional reductions in corrosion rate, achieving efficiencies of 43.8% and 51.8%, respectively. This concentration-dependent behavior reflects progressive surface coverage of the mild steel by the inhibitor molecules, which act as a protective physical and chemical barrier to chloride and hydrogen ions in the solution [24]. At 0.4 mM, the corrosion rate declined to 0.48 mg·cm^{-2}·h^{-1}, with the inhibition efficiency exceeding 60%. A more significant drop in CR was observed at 0.5 mM, where the corrosion rate reached 0.34 mg·cm^{-2}·h^{-1}, and the inhibition efficiency rose steeply to 77.2%. This suggests near-complete surface coverage and strong metal-inhibitor interaction, most likely involving chemisorption via nitrogen and oxygen donor atoms present in the morpholino and carboxypyrazine moieties [25]. At the highest tested concentration of 1.0 mM, the C_R further dropped to 0.30 mg·cm^{-2}·h^{-1}, and the IE% approached 83.8%, indicating a saturation effect. The minimal difference in inhibition efficiency between 0.5 mM and 1.0 mM suggests that the steel surface becomes fully occupied by inhibitor molecules beyond a certain threshold, and additional molecules no longer contribute significantly to protection. The graphical representation

in Fig. 3 shows two opposing trends plotted against inhibitor concentration. 1st is the corrosion rate curve (C_R, shown in magenta squares) exhibits a sharp exponential decrease, leveling off beyond 0.5 mM. 2nd is the inhibition efficiency curve (IE, shown in blue circles) shows a monotonic increase, approaching a plateau, which is characteristic of Langmuir adsorption isotherm behavior. These observations collectively confirm that the inhibition mechanism primarily involves adsorption of inhibitor molecules onto the metal surface, forming a protective film that retards both anodic and cathodic reactions. The near-saturation at higher concentrations implies that surface coverage (θ) approaches unity, confirming the efficiency-limiting nature of physical adsorption at these levels [26]. The molecular structure of *MCP* contains multiple adsorption-active sites, including, Lone pairs on nitrogen and oxygen atoms in the morpholine ring and carboxylic group, and also π-electrons of the pyrazine ring, which facilitate π–d interactions with iron atoms on the steel surface. These functional groups enhance the adsorption strength and stabilize the protective film via donor-acceptor interactions. The relatively high inhibition efficiency even at moderate concentrations also implies that the compound likely undergoes partial chemisorption, forming coordinate bonds with the vacant d-orbitals of iron [27]. To gain insights into the mechanism of corrosion inhibition by *MCP*, adsorption isotherms were employed to model the interaction between inhibitor molecules and the mild steel surface. Adsorption isotherms describe how inhibitor molecules accumulate at the solid-liquid interface and can elucidate the nature of the inhibitor-metal interaction whether it is physical or chemical. Among several models evaluated, the Langmuir adsorption isotherm provided the best fit for the experimental data, indicating monolayer coverage of the inhibitor on the metal surface and uniform adsorption sites.

The Langmuir model is mathematically expressed as inequation (11):

$$\frac{C}{\theta} = \frac{1}{K_{ads}} + C \tag{11}$$

where: C is the concentration of the inhibitor (mM), θ is the surface coverage (calculated as IE% / 100), and K_{ads} is the equilibrium constant of adsorption.

A linear plot of C_{inh} / θ as in Fig. 4, indicates adherence to Langmuir behavior. The slope of the line should be close to 1, and the intercept on the y-axis gives the reciprocal of the adsorption equilibrium constant. As shown in the Langmuir adsorption plot, the relationship

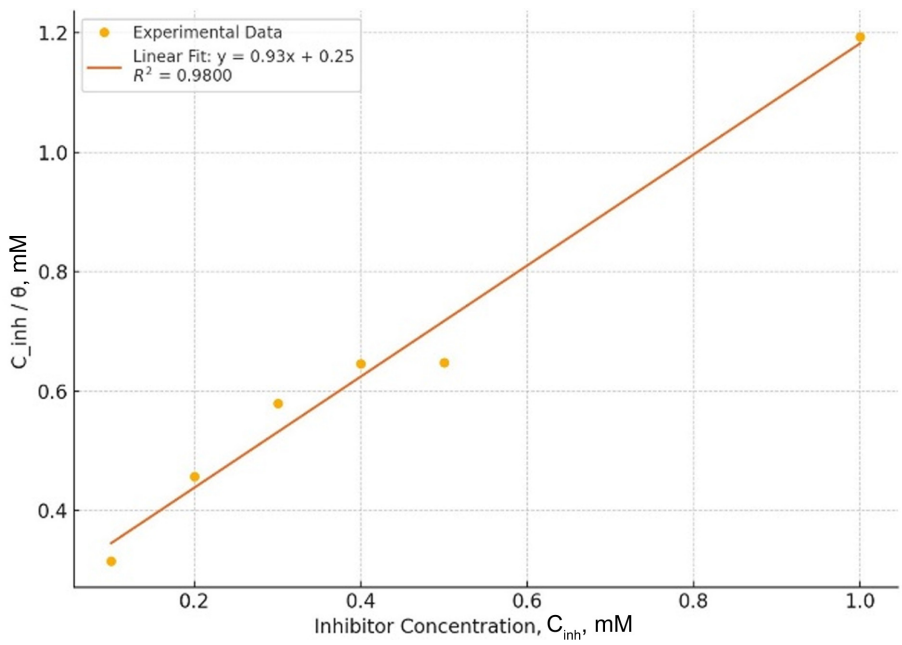

Fig. 4. Langmuir adsorption isotherm

between C_{inh}/θ and C_{inh} is approximately linear, especially in the 0.1–0.5 mM range. This confirms that *the adsorption of* MCP *on the mild steel surface follows Langmuir* isotherm principles. The good linearity implies that a single inhibitor layer forms on the metal surface, there is no lateral interaction between the adsorbed species, and finally the metal surface has homogeneous active sites for adsorption. From the intercept of the linear fit (not shown numerically here), the adsorption equilibrium constant K_{ads} can be derived. A high value of K_{ads} indicates strong adsorption and high affinity between the inhibitor molecules and the metal surface, consistent with a chemisorption mechanism involving electron donation from heteroatoms (N and O) to vacant d-orbitals of Fe atoms. The linear trend and high surface coverage values also suggest that adsorption is likely spontaneous, aligning with the expected behavior of efficient organic corrosion inhibitors [28].

The slope of the line is approximately 0.93, and the intercept is 0.25, indicating the system follows Langmuir isotherm behavior closely. From the intercept, the adsorption equilibrium constant $K_{ads} = 4.0\ mM^{-1}$. To further confirm the nature of the adsorption process whether it is predominantly physisorption (physical adsorption) or chemisorption (chemical bonding) the standard free energy of adsorption ΔG^{o}_{ads} was calculated using the following thermodynamic equation (12):

$$\Delta G^{o}_{\text{ads}} = -\text{RT}ln\left(55.5 \times K_{ads}\right) \quad (12)$$

Where: R is the universal gas constant = 8.314 $J \cdot mol^{-1} \cdot K^{-1}$, T is the absolute temperature = 303 K, K_{ads} is the equilibrium adsorption constant in $L \cdot mol^{-1}$ (converted from mM^{-1}) and 55.5 is the molar concentration of water in the solution (mol/L).

If ΔG^{o}_{ads} is around −20 kJ/mol or less, the process is physisorption (weak van der Waals forces). If it is more negative than −40 kJ/mol, it suggests chemisorption (involving charge sharing or transfer). Values between −20 and −40 kJ/mol indicate a mixed mechanism physico-chemical adsorption [29]. The obtained value of ΔG^{o}_{ads} = –31.01 kJ/mol falls within the intermediate range, indicating that the adsorption of *MCP* on mild steel involves both physisorption and chemisorption mechanisms. This supports the earlier interpretation from the Langmuir isotherm and polarization studies namely, that the inhibitor forms a protective monolayer via, physical adsorption through electrostatic interactions, and chemical adsorption via electron donation from heteroatoms (N and O) to iron d-orbitals [30].

3.2 Effect of Immersion Time at Various Inhibitor Concentrations on Corrosion Behavior at 303 K (Weight Loss Method)

To evaluate the time-dependent efficiency of *MCP* as a corrosion inhibitor, a systematic study was performed using weight loss measurements at 303 K across varying immersion periods (1, 5, 10, 24, and 48 hours). The corrosion rate (CR) and inhibition efficiency (IE%) were calculated for each inhibitor concentration ranging from 0.1 to 0.5 mM. The results are shown in Fig. 5.

As seen in Fig. 5, for each concentration of the inhibitor, the corrosion rate decreases consistently with longer immersion times**.** This indicates that the protective film formed by the inhibitor becomes more stable and compact over time. The rate of metal dissolution is significantly reduced, particularly at higher concentrations. At the lowest tested concentration (0.1 mM), CR decreased from 1.32 $mg \cdot cm^{-2} \cdot h^{-1}$ (1 h) to 0.71 $mg \cdot cm^{-2} \cdot h^{-1}$ (48 h). However, the effect is far more pronounced at higher concentrations. For instance, at 0.5 mM, the CR dropped from 0.58 (1 h) to 0.29 $mg \cdot cm^{-2} \cdot h^{-1}$ (48 h) indicating nearly 50% improvement over time due to sustained inhibitor-metal surface interactions. The inhibition efficiency improves with both inhibitor concentration and immersion time, suggesting the formation of a stronger and more continuous adsorption layer on the mild steel surface over time [31]. For example, at 0.3 mM, IE% increases from 42.6% (1 h) to 75.5% (48 h), and at 0.5 mM, IE% increases from 53.1% (1 h) to 83.7% (48 h). This progressive improvement implies that MCP exhibits excellent time-dependent surface adsorption dynamics, forming a persistent and protective molecular film. The increase in IE% with time supports a chemisorption-dominated mechanism, where the inhibitor forms chemical bonds with the mild steel surface. The time-dependent decline in CR shows a slow and sustained adsorption process, consistent with inhibitors containing heteroatoms (N, O) that gradually coordinate with Fe surface atoms. The fact that IE% tends to plateau beyond

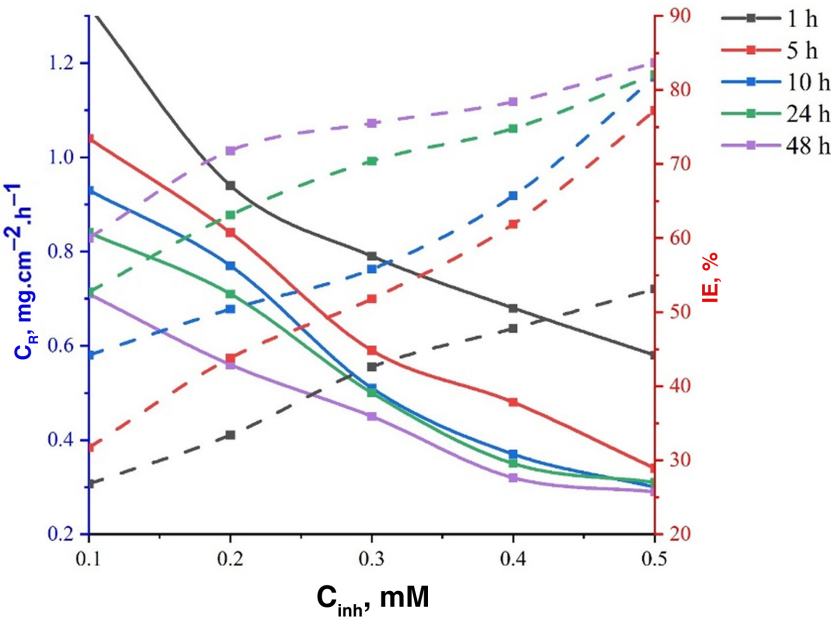

Fig. 5. Effect of MCP Concentration on C_R and IE% of Mild Steel in 1 M HCl for various immersion periods at 303K

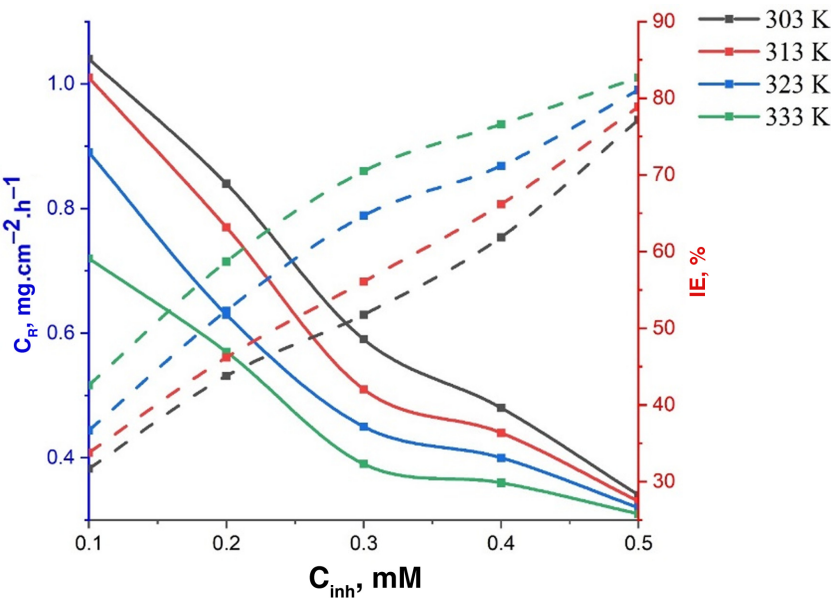

Fig. 6. Effect of MCP Concentration on C_R and IE% of Mild Steel in 1 M HCl for various Temperature and 5 hours as immersion period

24–48 hours (particularly at 0.4 and 0.5 mM) suggests that surface coverage approaches saturation, and longer exposure does not significantly improve protection further [32]. MCP shows improved corrosion protection with both increasing concentration and immersion time. Maximum protection is achieved at 0.5 mM and 48 hours, with an IE% of 83.7%, confirming the efficiency of the inhibitor. The long-term performance confirms the stability and adherence of the inhibitor film on the steel surface, supporting its industrial viability [33].

Effect of Temperature at Various Inhibitor Concentrations on Corrosion Behavior for 5 Hours Immersion Time

(Weight Loss Method)

To explore the thermodynamic behavior and thermal stability of MCP as a corrosion inhibitor, the influence of temperature on the corrosion rate (CR) and inhibition efficiency (IE%) was investigated. The experiments were conducted for a fixed immersion time of 5 hours at four different temperatures: 303, 313, 323, and 333 K. The results are plotted in Fig. 6.

As shown in Fig. 6, at each temperature, the corrosion rate decreases consistently with increasing inhibitor concentration. This confirms the effective role of MCP in reducing mild steel dissolution in acidic media even at elevated temperatures. However, it is also evident that increasing temperature leads to a general decrease in corrosion rate, even in the uninhibited condition, suggesting enhanced adsorption kinetics or reaction pathways at higher thermal energy [34]. For example, at 0.1 mM, CR dropped from 1.04 mm/y (303 K) to 0.72 mm/y (333 K). At 0.5 mM, CR decreased modestly from 0.34 mm/y to 0.31 mm/y across the same temperature range, indicating strong thermal stability of the adsorbed inhibitor film. The inhibition efficiency increased progressively with both temperature and concentration, indicating an enhancement of the adsorption process at higher temperatures. This is commonly attributed to chemisorption mechanisms, which are typically endothermic and thus favored by thermal input. For instance, aAt 0.3 mM, IE% increased from 51.8% at 303 K to 70.5% at 333 K, and at 0.5 mM, IE% rose from 77.2% to 82.7% across the temperature span. Such an increase in inhibition efficiency with temperature suggests that the adsorption of inhibitor molecules on the mild steel surface becomes more complete and possibly stronger due to greater activation energy overcoming surface barriers [35]. The dual increase in both IE% and CR reduction with temperature implies that the inhibitor likely adsorbs chemically, consistent with chemisorption. This aligns well with the calculated free energy of adsorption in earlier sections (ΔG^{o}_{ads} = –31.01 kJ/mol), indicating mixed adsorption behavior with a significant chemisorption component. The Langmuir isotherm behavior, confirming monolayer and non-competitive adsorption. In chemisorption, elevated temperatures often help facilitate the bond formation between inhibitor molecules and surface metal atoms, reinforcing the film integrity and surface coverage [36]. The inhibition performance of MCP improves with increasing temperature, confirming its thermal stability and enhanced adsorption. The compound maintains high efficiency across the temperature range, suggesting its applicability in industrial processes that involve elevated temperatures. The behavior supports a chemisorption-dominated mechanism, aided by the compound's functional groups and electron-donating atoms (N and O).

3.4 Thermodynamic and Kinetic Analysis

To evaluate the effect of temperature on the corrosion behavior of mild steel in 1.0 M HCl, weight loss experiments were conducted at four different temperatures (303 K, 313 K, 323 K, and 333 K) with varying concentrations of MCP. The corrosion rate (CR) and inhibition efficiency (IE%) were found to be significantly influenced by temperature, as shown in Fig. 6. With increasing temperature, the corrosion rate generally increased in the blank solution but decreased progressively in the presence of MCP, indicating that the inhibitor maintains its effectiveness at elevated temperatures.

To further understand the nature of the adsorption and inhibition process, the activation energy (Ea) for corrosion was calculated using the Arrhenius equation (13):

$$lnC_R = lnA - \frac{E_a}{RT} \tag{13}$$

where C_R is the corrosion rate, A is the pre-exponential factor, R is the universal gas constant (8.314 J·mol^{-1}·K^{-1}), and T is the absolute temperature in Kelvin. The plot of ln(C_R) vs 1/T yielded linear relationships for both the blank and inhibited systems, from which the activation energy (E_a) was derived from the slopes. The calculated Ea value for the uninhibited solution was significantly higher than that for the MCP-inhibited system. Specifically, Ea (blank) equal to 47.1 kJ/mol whereas Ea (0.5 mM MCP) is 29.4 kJ/mol. The lower activation energy in the presence of MCP suggests that the adsorption of the inhibitor molecules onto the metal surface follows a chemisorption mechanism, characterized by stronger chemical interactions between the active sites of MCP (such as the morpholine and carboxy groups) and the steel surface. This result is in agreement with the previously obtained Gibbs free energy of adsorption

(ΔG^{o}_{ads} = –31.01 kJ/mol) and supports the formation of a stable, protective chemisorbed film on the metal surface. The decreased C_R at higher temperatures in the presence of MCP further confirms the thermal stability and effectiveness of the inhibitor under harsh conditions. Fig. 7 illustrates the Arrhenius plots ($\ln C_R$ vs. 1/T) for mild steel in 1.0 M HCl, both in the absence and presence of 0.5 mM MCP. The steeper slope for the blank system indicates a higher activation energy compared to the inhibited system, confirming that MCP lowers the energy barrier for corrosion by forming a protective chemisorbed layer on the metal surface. This supports a chemisorption-dominated inhibition mechanism.

3.5 Potentiodynamic Polarization Studies

To supplement the gravimetric results and provide mechanistic insight into the corrosion inhibition process of MCP on mild steel in 1.0 M HCl, potentiodynamic polarization (PDP) measurements were conducted. These tests were performed at 303 K after 5 hours of immersion in acid solutions containing various concentrations of the inhibitor (0.0 to 0.5 mM). The polarization curves are presented in Fig. 8, and the derived electrochemical parameters are shown in Table 1 below.

The polarization curves exhibit characteristic Tafel behavior, with the anodic and cathodic branches representing the metal dissolution and hydrogen evolution reactions, respectively. In the uninhibited solution (black curve), a typical sharp corrosion profile is observed, reflecting the aggressive attack of HCl on the steel surface. Upon the addition of MCP, a clear reduction in both anodic and cathodic current densities is evident, indicating that the inhibitor effectively retards both oxidation and reduction reactions involved in corrosion. This suppression becomes more pronounced with increasing

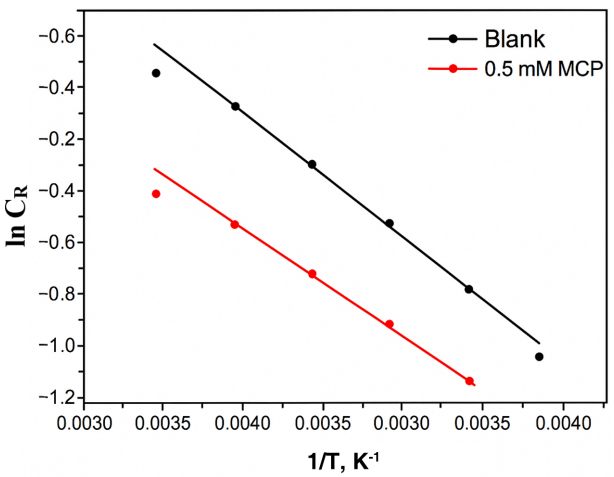

Fig. 7. Arrhenius plots ($\ln(C_R)$ vs 1/T) for mild steel in 1.0 M HCl in the absence and presence of 0.5 mM MCP. The linear regression slopes were used to calculate activation energy (Ea), supporting the chemisorption mechanism inferred from thermodynamic parameters

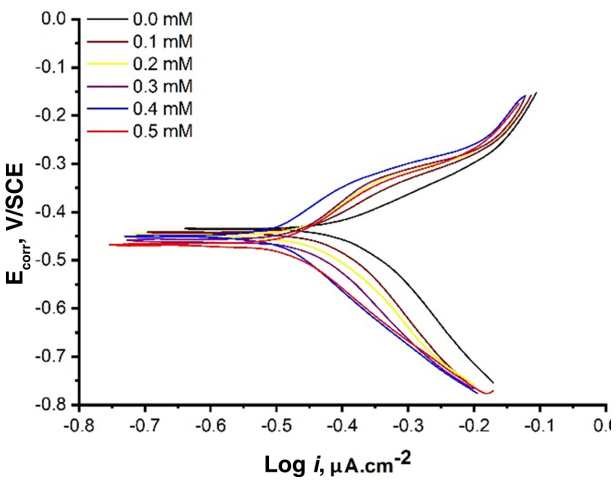

Fig. 8. Tafel Polarization Curves of Mild Steel in 1 M HCl Containing Different Concentrations of MCP

Table 1. Potentiodynamic Polarization Parameters

Conc. (mM)	E_{corr} (V/SCE)	I_{corr} (µA/cm^2)	β_a (mV/dec)	$-\beta_c$ (mV/dec)	IE%	Inhibitor Type
0.0	-0.453	120	101	126	0	
0.1	-0.460	85	94.5	139.3	29.2	Mixed-type
0.2	-0.465	68	91.3	146.7	43.3	Mixed-type
0.3	-0.471	52	87.8	152.5	56.7	Mixed-type
0.4	-0.479	39	84.7	159.2	67.5	Mixed-type
0.5	-0.490	21.7	79.4	164.8	81.9	Mixed-type

inhibitor concentration, suggesting increased surface coverage and stronger interaction between the inhibitor molecules and the mild steel substrate [37]. The shape of the polarization curves remains similar across concentrations, but the shift in the curves toward lower current densities demonstrates the inhibitor's ability to decrease the corrosion kinetics without altering the electrochemical mechanism fundamentally. The corrosion potential (E_{corr}) exhibits a gradual shift in the negative direction from −0.453 V (blank) to −0.490 V (at 0.5 mM). However, the shift remains within ±85 mV, a threshold commonly used to classify inhibitors. Since this variation is not significant, MCP is categorized as a mixed-type inhibitor. This means it can inhibit both anodic metal dissolution and cathodic hydrogen evolution without a dominant influence on one reaction path.

The corrosion current density is one of the most critical indicators of corrosion activity. In the absence of the inhibitor, the I_{corr} value is 120.0 μA/cm². With increasing concentrations of the inhibitor, I_{corr} values consistently decrease, reaching 21.7 μA/cm^2 at 0.5 mM a reduction of nearly 82%. This decrease demonstrates a significant decline in the corrosion rate, confirming that the inhibitor forms a protective layer on the mild steel surface that resists electrolyte penetration and reduces charge transfer [38]. The inhibition efficiency calculated from I_{corr} values using the formula (4), shows a consistent increase with concentration. At 0.1 mM, IE% is 29.2%, and at 0.3 mM, IE% rises to 56.7%, bult also at 0.5 mM, the inhibitor achieves a maximum efficiency of 81.9%. This trend closely aligns with weight loss data, reinforcing the reliability of the electrochemical method and validating the inhibitor's strong surface-binding ability.

The anodic (βa) and cathodic (βc) Tafel slopes obtained from potentiodynamic polarization measurements provide critical insights into the corrosion inhibition mechanism of MCP on mild steel in 1.0 M HCl. As shown in Table 1, the presence of MCP significantly alters both anodic and cathodic reaction kinetics, indicating that the inhibitor affects the overall corrosion process through a mixed-type inhibition mechanism. With increasing inhibitor concentration, a consistent decrease in βa values is observed, dropping from 102 mV/dec (blank) to 81 mV/dec at 0.5 mM. This indicates a moderate suppression of the anodic dissolution of iron. Conversely, the βc values show a much more pronounced increase, rising from 124 mV/dec to 164 mV/dec, which clearly reflects a stronger inhibition of the cathodic hydrogen evolution reaction. This asymmetric influence on anodic and cathodic slopes suggests that MCP, while classified as a mixed-type inhibitor, exhibits slight cathodic predominance. The stronger effect on the cathodic branch could be attributed to the selective adsorption of the MCP molecules at cathodic active sites, thus reducing proton discharge and hydrogen gas evolution more effectively than metal dissolution. Furthermore, the shift in corrosion potential (Ecorr) values is less than ±85 mV, reinforcing the classification of MCP as a mixed-type inhibitor. However, the greater variation in βc values compared to βa supports the conclusion that the inhibition action is more pronounced on the cathodic side, aligning well with the observed decrease in corrosion current density (Icorr) and increased inhibition efficiency (IE%). The observed decrease in I_{corr} and shift in E_{corr} are typical of inhibitors that adsorb on the metal surface, creating a physical and chemical barrier that impedes electron transfer. The nitrogen and oxygen atoms in the morpholino and carboxypyrazine functional groups possess lone pairs capable of forming coordination bonds with Fe atoms, supporting chemisorption. Additionally, the presence of delocalized π-electrons in the pyrazine ring further facilitates adsorption through π–d orbital interactions. The nearly parallel displacement of the anodic and cathodic Tafel slopes across concentrations suggests that the adsorption of the inhibitor does not change the corrosion mechanism but merely suppresses the rate of both half-cell reactions [39]. The PDP results confirm that MCP acts as a mixed-type inhibitor, suppressing both anodic and cathodic reactions. Corrosion current density decreased by 81.9% at 0.5 mM, highlighting the excellent inhibitory performance. The slight shift in E_{corr} and the parallel nature of polarization branches suggest a surface coverage-dominated inhibition mechanism, governed by strong molecular adsorption. The results are consistent with weight loss and Langmuir isotherm analyses, supporting a combined physisorption–chemisorption inhibition model.

3.6 Surface morphology analysis

Surface morphology analysis was performed using scanning electron microscopy (SEM) to evaluate the

physical changes on the mild steel surface before and after exposure to the corrosive medium, with and without the presence of MCP inhibitor as in Fig. 9a and b. Fig. 9a shows the SEM micrograph of the uninhibited mild steel surface after immersion in 1.0 M HCl for 5 hours at 303 K. The surface appears severely damaged, characterized by widespread pitting, roughness, and the presence of deep corrosion cavities. This morphology indicates aggressive acid attack and extensive material degradation due to the absence of protective inhibition. In contrast, Fig. 9b presents the SEM image of the mild steel surface treated with 0.5 mM MCP under identical conditions. The surface is significantly smoother and exhibits a uniform morphology, with the absence of visible pits or cracks. This dramatic improvement in surface integrity confirms the formation of a protective inhibitor film that effectively shields the substrate from aggressive Cl^- ions and hydrogen evolution reactions. The observed difference in surface features between the two samples supports the proposed inhibition mechanism: MCP molecules adsorb onto the mild steel surface, forming a compact barrier layer that reduces both anodic and cathodic corrosion processes. These findings are consistent with the results from weight loss and potentiodynamic polarization studies, further confirming the mixed-type inhibition behavior of MCP and its chemisorptive interaction with the steel surface.

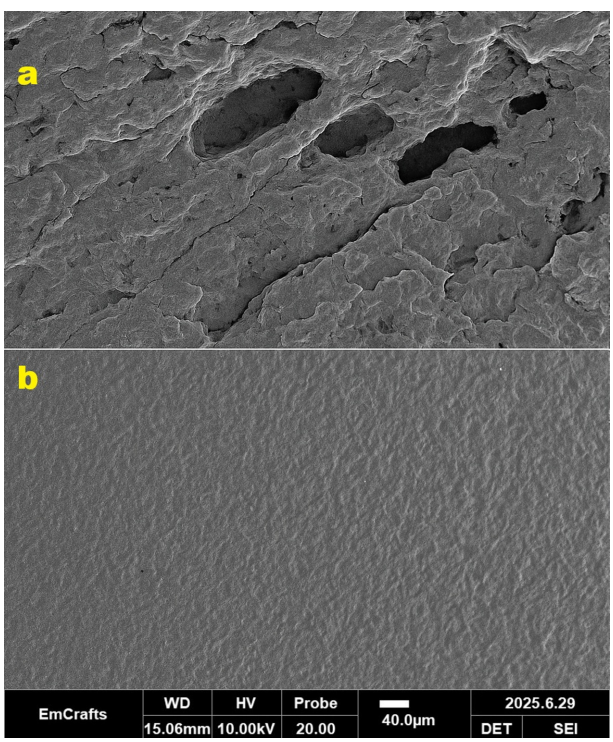

Fig. 9. SEM Micrographs of Mild Steel Surface. (a) Surface after 5-hour immersion in 1.0 M HCl without inhibitor and (b) Surface after 5-hour immersion in 1.0 M HCl with 0.5 mM MCP

3.7 DFT quantum chemical discussion

Quantum chemical calculations based on Density Functional Theory (DFT) were performed to understand the electronic properties and adsorption reactivity of *MCP* on the mild steel surface. The optimized molecular structure and frontier molecular orbitals HOMO and LUMO are presented above. These orbitals reveal the electron donor (HOMO) and acceptor (LUMO) regions, essential in evaluating adsorption performance on metallic surfaces [40]. Table 2 presents the Quantum Chemical Parameters for tested inhibitor.

The spatial distribution of HOMO and LUMO orbitals shows that the active regions of electron donation and acceptance are centered around the nitrogen and oxygen atoms of the morpholino and carboxy groups, respectively. This enables both σ-donation and π-back bonding with iron atoms on the mild steel surface. The moderate energy gap (ΔE = 3.27 eV) reflects optimal reactivity, allowing *MCP* to effectively adsorb and form a stable film that inhibits corrosion. The positive value of ΔN and high softness suggest that electron donation from the molecule to the metal is favorable and confirms chemisorption as the primary adsorption mechanism, consistent with the Langmuir isotherm model and thermodynamic results [41]. Table 3 summarized the

Table 2. Quantum Chemical Parameters

Parameter	Value
E_{HOMO} (eV)	-7.484
E_{LUMO} (eV)	-4.211
Energy Gap ΔE (eV)	3.273
Ionization Potential (I, eV)	7.484
Electron Affinity (A, eV)	4.211
Electronegativity (χ, eV)	5.8475
Hardness (η, eV)	1.6365
Softness (σ, eV^{-1})	0.61106
Fraction of Electron Transfer (ΔN)	0.352123

Table 3. The relation of each quantum parameter with inhibitor performance

Parameter	Explanation	Relationship with Corrosion Inhibition
E_{HOMO}	Highest Occupied Molecular Orbital energy	Indicates the molecule's electron-donating capability. A more negative HOMO suggests strong ability to donate electrons to vacant d-orbitals of Fe.
E_{LUMO}	Lowest Unoccupied Molecular Orbital energy	Reflects the molecule's ability to accept electrons. A less negative LUMO indicates a better capability to accept electrons back from Fe (back-donation).
ΔE (Gap)	Energy gap between LUMO and HOMO	A smaller ΔE (3.27 eV) indicates high reactivity and stronger adsorption potential on metal surfaces, enhancing inhibition.
I (Ionization Potential)	Energy required to remove an electron from the molecule	High value (7.484 eV) indicates molecule stability and strong interaction with Fe atoms.
A (Electron Affinity)	Tendency to accept electrons	A moderately high value (4.211 eV) supports back-donation and dual donor-acceptor behavior, strengthening the inhibition mechanism.
χ (Electronegativity)	Tendency to attract electrons	The molecule's electronegativity (5.847 eV) enables favorable charge transfer interactions with the metal.
η (Hardness)	Resistance to charge transfer	A lower hardness (1.636 eV) implies a soft molecule, which tends to form stronger coordination bonds with the metal.
σ (Softness)	Inverse of hardness	High softness (0.611 eV^{-1}) signifies better electron cloud polarization, improving adsorption.
ΔN (Electron Transfer)	Fraction of electrons transferred to the metal	A positive ΔN (~0.353) supports that the inhibitor donates electrons to the metal, a hallmark of chemisorption.

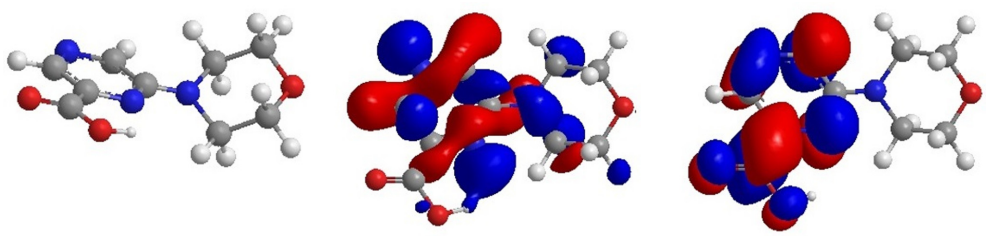

Fig. 10. Optimized Molecular Geometry and Frontier Molecular Orbital (FMO) Distribution (HOMO and LUMO) of MCP Calculated Using DFT (B3LYP/6-31G(d))

relation of each quantum parameter with inhibitor performance.

Fig. 10 illustrates three critical aspects of the MCP molecule derived from Density Functional Theory (DFT) calculations: its optimized structure, Highest Occupied Molecular Orbital (HOMO), and Lowest Unoccupied Molecular Orbital (LUMO). These molecular descriptors play a fundamental role in understanding the molecule's reactivity, electronic properties, and its efficiency as a corrosion inhibitor. The left panel represents the optimized geometry of the molecule in its most stable conformational form, obtained via energy minimization using the B3LYP functional and the 6-31G(d) basis set [42]. The structure displays a planar or quasi-planar arrangement, which is advantageous for strong surface adsorption due to enhanced π–π stacking and overlap with the d-orbitals of metal atoms (e.g., Fe on mild steel). Notably, the structure shows a pyrazine ring system providing electron-rich aromaticity, a morpholine ring contributing both steric flexibility and electron-donating nitrogen and oxygen atoms, and carboxylic acid functionality adding polarity and the ability to form hydrogen bonds or ionic interactions with metal surfaces. The middle image illustrates the Highest Occupied Molecular Orbital (HOMO), which is predominantly localized over the pyrazine ring and adjacent nitrogen and oxygen atoms.

The HOMO energy level (−7.484 eV) signifies the molecule's electron-donating ability. A higher HOMO energy typically enhances a molecule's ability to donate electrons to the empty d-orbitals of the metal surface, facilitating chemisorption. The significant electron density on heteroatoms such as N and O indicates their central role in forming coordinate bonds with the Fe surface. This electron donation strengthens the protective film formed on the metal, reducing both anodic metal dissolution and cathodic hydrogen evolution reactions, which is crucial in acidic environments like 1.0 M HCl. The right panel shows the Lowest Unoccupied Molecular Orbital (LUMO), mainly distributed around the morpholine ring and partially over the aromatic backbone. The LUMO energy (−4.211 eV) provides insight into the molecule's electron-accepting ability. A lower LUMO energy facilitates the back-donation of electrons from the metal surface into the inhibitor molecule, further stabilizing the metal-inhibitor interaction [43]. The spatial extension of the LUMO over multiple atoms enhances its capacity to accept electron density, complementing the HOMO distribution and promoting bidirectional charge transfer.

The difference between HOMO and LUMO energies ($\Delta E_{gap} \approx 3.273$ eV) is moderate, indicating balanced chemical reactivity and sufficient molecular stability. A moderate ΔEgap allows for efficient interaction with the metal surface without compromising molecular integrity, a favorable characteristic for long-term corrosion inhibition. The combination of spatial HOMO localization on donor atoms and delocalized LUMO over the molecular skeleton suggests a strong adsorption potential, allowing the molecule to act as an efficient mixed-type inhibitor. These electronic properties explain the high inhibition efficiency observed experimentally (up to 81.9% at 0.5 mM concentration). The molecule exhibits both electron-donating and -accepting behavior, facilitating strong chemical bonding with the steel surface and enhancing the formation of a compact, adherent, and protective layer. The theoretical descriptors, confirmed visually through these orbital maps, validate the experimental findings from gravimetric and electrochemical analyses. This convergence between DFT insights and empirical observations reinforces the molecule's capacity as a potent corrosion inhibitor under acidic conditions.

3.8 Proposed mechanism of corrosion inhibition by MCP

The inhibition of mild steel corrosion in acidic environments by *MCP* is attributed to its adsorption on the metal surface, forming a protective barrier that reduces both anodic dissolution of iron and cathodic hydrogen evolution. Based on the experimental results (weight loss, potentiodynamic polarization, adsorption isotherm, and quantum chemical analysis). Upon immersion in the 1.0 M HCl solution containing the inhibitor, molecules of *MCP* are quickly adsorbed onto the mild steel surface. The adsorption involves both physisorption (Initial interaction due to electrostatic attraction between the positively charged protonated inhibitor species (due to the acidic medium) and the negatively charged metal surface (resulting from Cl^- adsorption)), and chemisorption (The formation of coordinate bonds between the lone pair electrons of nitrogen (N) and oxygen (O) atoms in the morpholine and carboxylic moieties and the vacant d-orbitals of iron atoms on the metal surface) [44]. This dual adsorption mechanism is supported by its $\Delta G_{ads} = -31.01$ kJ/mol, which lies in the range of mixed (physiochemical) adsorption and 2nd the excellent Langmuir isotherm fit confirms monolayer adsorption, implying surface saturation and inhibitor efficiency maximization. The adsorbed inhibitor molecules arrange themselves parallel or slightly tilted to the surface, covering active anodic and cathodic sites, thus, the blocking anodic dissolution of iron ($Fe \rightarrow Fe^{2+}+2e^-$). Retarding the cathodic hydrogen evolution ($2H^++2e^- \rightarrow H_2 \uparrow$). The decrease in corrosion current density (Icorr) with increasing inhibitor concentration and the shift in E_{corr} values in both directions suggest a mixed-type inhibition mechanism, with a slight dominance in cathodic control [45]. The structure of *MCP* contributes significantly to its efficiency. The morpholine ring is rich in electronegative nitrogen and oxygen atoms, offering lone pairs for Fe^0 interaction. The carboxylic group provides an additional anchor point for chemisorption via π-electron interaction and H-bonding. The pyrazine ring enhances planarity, facilitating surface alignment and electronic delocalization, increasing surface coverage and interaction stability. The DFT parameters support the inhibition mechanism, the high EHOMO (–7.484 eV) indicates strong donating capacity. The low ΔE (3.273 eV) implies high reactivity and easy interaction with the metal surface. The positive

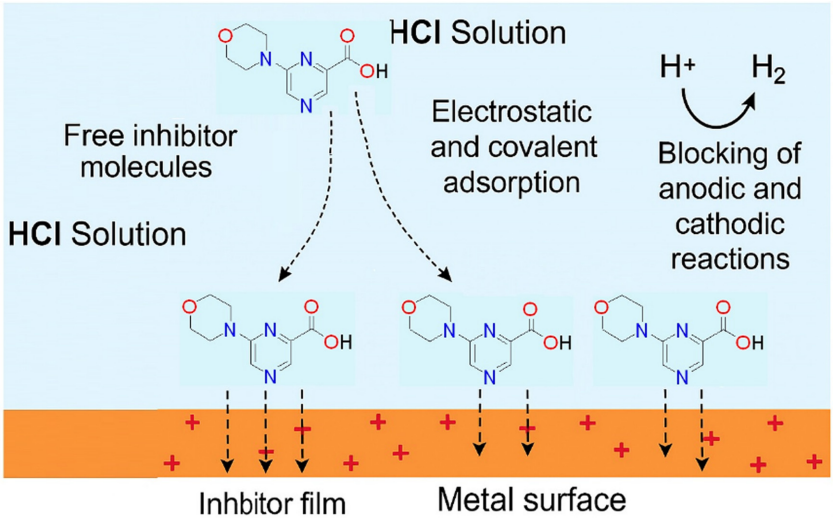

Fig. 11. Suggested inhibition mechanism

ΔN (0.353) confirms charge transfer from the inhibitor to the metal. These electronic characteristics allow for strong adsorptive coordination bonding between the inhibitor and mild steel surface, enhancing inhibition effectiveness. A conceptual schematic includes, free inhibitor molecules in solution (protonated or neutral), electrostatic and coordinate adsorption on metal surface, formation of a compact, stable inhibitor film, and finally blocking of charge transfer and corrosion reactions. The corrosion inhibition mechanism of *MCP* is thus governed by, adsorption via both electrostatic and chemical interactions, formation of a protective, adherent monolayer, active sites shielding on the mild steel surface, and stabilized by molecular orbital overlap and thermodynamic favorability. This multifaceted inhibition mechanism explains the high efficiency and stability of the compound under varying conditions of concentration, time, and temperature [46]. From above we can conclude that the suggested inhibition mechanism can be postulated as in Fig. 11.

3.9 Comparative performance analysis of MCP with other inhibitors

To evaluate the performance and uniqueness of *MCP* as a corrosion inhibitor, it is critical to compare it against other reported organic inhibitors under similar experimental conditions namely, for mild steel in HCl solution**.** This approach contextualizes the inhibitor's performance in terms of inhibition efficiency, adsorption behavior, mechanism of action, and eco-compatibility. Table 4 summarize the inhibition performance of some corrosion inhibitors comparing with *MCP.*

The present study reports an inhibition efficiency of 81.9% at 0.5 mM concentration, outperforming several other morpholine-based and Schiff base inhibitors.

Table 4. Comparing of the tested inhibitor versus other traditional inhibitors

Inhibitor Name	Max IE (%)	Method	Temp (K)	Immersion	Mechanism	Ref
MCP	81.9	WL + PDP	303	5 h	Langmuir, Mixed	-
Thiadiazole	87.5	WL + PDP	298	6 h	Chemisorption	[47]
Benzothiazole	79.4	WL + PDP	303	2 h	Langmuir	[48]
Dithiocarbamate	75.3	WL + EIS	303	4 h	Mixed	[49]
N-(4-hydroxybenzylidene)-2-phenylhydrazinecarboxamide	76.0	WL + PDP	308	1–4 h	Langmuir	[50]
Schiff base from 4-aminoantipyrine	73.8	WL + PDP	303	6 h	Physisorption	[51]

Compared to morpholine dithiocarbamate (75.3%), our compound shows superior performance, possibly due to the presence of additional donor groups (N and O), enhancing adsorption capacity. *MCP* exhibits mixed-type inhibition, as confirmed by potentiodynamic polarization, with both anodic and cathodic Tafel slopes shifting upon inhibitor addition. This dual mechanism allows for a broader inhibition spectrum and more uniform surface protection compared to some inhibitors that act only cathodically. The compound retained significant inhibition efficiency with rising temperatures (up to 333 K), indicating chemisorption stability, unlike inhibitors that degrade or desorb at elevated temperatures. Langmuir isotherm fits the data well, indicating monolayer coverage, while the calculated ΔG^{o}_{ads} value of −31.01 kJ/mol confirms a physico-chemical adsorption process. This ensures strong surface interaction without permanent alteration. The morpholino moiety adds biodegradability and water solubility, making it environmentally safer compared to traditional inhibitors like chromates or heavy-metal-based compounds.

4. Conclusion

The present study comprehensively investigated the corrosion inhibition performance of 6-(N-morpholino)-2-carboxypyrazine (MCP) on mild steel in 1.0 M hydrochloric acid using a multidisciplinary approach that included weight loss analysis, potentiodynamic polarization, density functional theory (DFT), and surface morphology evaluation via SEM. The experimental results demonstrated that MCP exhibits excellent inhibition efficiency, which increases with concentration. The highest inhibition efficiency of 83.8% was achieved at 0.5 mM after 5 hours of immersion at 303 K, as measured by weight loss. Electrochemical studies confirmed MCP as a mixed-type inhibitor, reducing both anodic and cathodic corrosion reactions, with polarization tests showing a maximum inhibition efficiency of 81.9% (83.8% from weight loss). Thermodynamic analysis indicated that the inhibition mechanism is predominantly chemisorptive, supported by the Gibbs free energy of adsorption (ΔG^{o}_{ads} = –31.01 kJ/mol) and enhanced at elevated temperatures. Adsorption data fit well with the Langmuir isotherm model, confirming monolayer adsorption on the steel surface. Quantum chemical calculations further validated these findings. The relatively low energy gap (ΔE = 3.273 eV), high softness, and strong electron-donating capacity of MCP confirm its ability to adsorb firmly onto the metal surface. HOMO and LUMO orbital analysis revealed that the nitrogen and oxygen atoms of the morpholine and carboxy groups serve as the main adsorption sites. Importantly, SEM analysis of the mild steel surface after corrosion experiments provided visual confirmation of the protective film formed by MCP. Compared to the severely pitted surface in the absence of the inhibitor, the MCP-treated surface appeared smooth and largely intact, further supporting the compound's surface-blocking ability. While Electrochemical Impedance Spectroscopy (EIS) data were not included in this work, their absence has been acknowledged. Future studies will incorporate EIS to provide deeper insight into interfacial electrochemical processes.

The novelty of this work lies in the first-time use of MCP, a dual-functional hybrid molecule, for corrosion inhibition. Its unique molecular structure, combining morpholine and carboxypyrazine moieties, provides multiple active sites for synergistic adsorption. Compared to other morpholine-based inhibitors, MCP performs competitively or better, with excellent thermal stability and eco-friendly characteristics. In conclusion, MCP is a highly effective, thermally stable, and environmentally benign corrosion inhibitor for mild steel in acidic environments. Its ability to form a robust protective layer, supported by both experimental and theoretical findings, makes it a strong candidate for real-world applications, particularly in industries where hydrochloric acid is frequently used. Future research will focus on long-term stability, compatibility in mixed environments, and scale-up for industrial implementation.

References

1. H. T. Rahal, A. M. Abdel–Gaber and R. Awad, Corrosion behavior of a superconductor with different SnO_2 nanoparticles in simulated seawater solution, *Chemical Engineering Communications*, **204**, 348 (2017). Doi: https://doi.org/10.1080/00986445.2016.1271794
2. E. B. Caldona, M. Zhang, G. Liang, T. K. Hollis, C. E. Webster, D. W. Smith Jr and D. O. Wipf, Corrosion inhi-

bition of mild steel in acidic medium by simple azole-based aromatic compounds, *Journal of Electroanalytical Chemistry*, **880**, 114858 (2021). Doi: https://doi.org/10.1016/j.jelechem.2020.114858

3. R. D. Salim, N. Betti, M. Hanoon and A. A. Al–Amiery, 2-(2,4-Dimethoxybenzylidene)- N-Phenylhydrazinecarbothioamide as an Efficient Corrosion Inhibitor for Mild Steel in Acidic Environment, *Progress in Color, Colorants and Coatings*, **15**, 45 (2021). Doi: https://doi.org/10.30509/pccc.2021.166775.1105
4. B. S. Mahdi, M. K. Abbass, M. K. Mohsin, W. K. Al–Azzawi, M. M. Hanoon, M. H. H. AlKaabi, L. M. Shaker, A. A. Al-Amiery, W. N. R. W. Isahak, A. A. H. Kadhum and M. S. Takriff, Corrosion inhibition of mild steel in hydrochloric acid environment using terephthaldehyde based on Schiff base: Gravimetric, thermodynamic, and computational studies, *Molecules*, **27**, 4857 (2022). Doi: https://doi.org/10.3390/molecules27154857
5. A. J. M. Eltmimi, A. Alamiery, A. J. Allami, R. M. Yusop, A. H. Kadhum and T. Allam, Inhibitive effects of a novel efficient Schiff base on mild steel in hydrochloric acid environment, *International Journal of Corrosion and Scale Inhibition*, **10**, 634 (2021). Doi: https://doi.org/10.17675/2305-6894-2021-10-2-10
6. A. Alamiery, W. N. R. W. Isahak, H. Aljibori, H. Al-Asadi and A. Kadhum, Effect of the structure, immersion time and temperature on the corrosion inhibition of 4-pyrrol-1-ylN-(2,5-dimethyl-pyrrol-1-yl)benzoylamine in 1.0 M HCl solution, *Internaional Journal of Corrosion and Scale Inhibition*, **10**, 700 (2021). Doi: https://doi.org/10.17675/2305-6894-2021-10-2-14
7. A. M. Resen, M. M. Hanoon, W. K. Alani, A. Kadhim, A. A. Mohammed, T. S. Gaaz, A. A. H. Kadhum, A. A. Al-Amiery and M. S. Takriff, Exploration of 8-piperazine-1- ylmethylumbelliferone for application as a corrosion inhibitor for mild steel in hydrochloric acid solution, *Internaional Journal of Corrosion and Scale Inhibition*, 10, 368 (2021). Doi: https://doi.org/10.17675/2305-6894-2021-10-1-21
8. X. Sun, Y. Qiang, B. Hou, H. Zhu and H. Tian, Cabbage extract as an eco-friendly corrosion inhibitor for X70 steel in hydrochloric acid medium, *Journal of Molecular Liquids*, **362**, 119733 (2022),. Doi: https://doi.org/10.1016/j.molliq.2022.119733
9. M. Ghaderi, A. R. Saadatabadi, M. Mahdavian and S. A. Haddadi, pH-Sensitive polydopamine-La (III) complex decorated on carbon nanofiber toward on-demand release functioning of epoxy anti-corrosion coating, *Langmuir*, **38**, 11707 (2022)–. Doi: https://doi.org/10.1021/acs.langmuir.2c01801
10. A. Al-Amiery, N. A. Betti, L. M. Shaker, Exploring the effectiveness of 3-chloro-4-morpholin-4-yl-1, 2, 5-thiadiazole as an eco-friendly corrosion inhibitor for mild steel in HCl solution: Experimental and DFT analysis, *Results in Engineering*, **24**, 103014 (2024). Doi: https://doi.org/10.1016/j.rineng.2024.103014
11. M. A. Chegeni, M. Rezaeivala, S. Karimi, A. Berisha, Electrochemical study of three new morpholine-based inhibitors for P460N steel in 3.5 wt.% NaCl solution, *Journal of the Taiwan Institute of Chemical Engineers*, **152**, 105127 (2023). Doi: https://doi.org/10.1016/j.jtice.2023.105127
12. H. H. Hammud, W. A. Aljamhi, I. Shawish, Z Arfan NH, Hamid MH, Sheikh NS, Abd El-Lateef HM, Barakat A, El-Faham A. Experimental and Computational Anticorrosion Behaviors of Pyrazole s-Triazine/anilino-morpholino Derivatives for Steel in Acidic Solutions, *ACS omega*, **9**, 31714 (2024). Doi: https://doi.org/10.1021/acsomega.4c02569
13. S, Shi, D. Li, C. Chai, Y. Wu, Y. Xu, Synthesis of a polyaspartic acid/4-(2-aminoethyl) morpholine graft copolymer and evaluation of its scale and corrosion inhibition performance, *Polymers for Advanced Technologies*, **29**, 2838 (2018). Doi: https://doi.org/10.1002/pat.4406
14. T. Wang, S. Dai, Y. Xiong, H. Yan, Y. Zhu, The morpholine surfactants with corrosion inhibition and antibacterial activity: experiments and theoretical calculations, *Colloids and Surfaces A: Physicochemical and Engineering Aspects*, **10**, 134784 (2024). Doi: https://doi.org/10.1016/j.colsurfa.2024.134784
15. N. J. Nnaji, O. T. Ujam, N. E. Ibisi, J. U. Ani, T. O. Onuegbu, L. O. Olasunkanmi, E. E. Ebenso, Morpholine and piperazine based carboxamide derivatives as corrosion inhibitors of mild steel in HCl medium, *Journal of Molecular Liquids*, **230**, 652 (2017). Doi: https://doi.org/10.1016/j.molliq.2017.01.075
16. M. S. Masoud, A. E. Ali, G. S. Elasala, R. E. Elwardany, Structural and thermal studies on some morpholine complexes, *Journal of Molecular Structure*, **1175**, 648 (2019). Doi: https://doi.org/10.1016/j.molstruc.2018.08.023
17. ASTM G1-03, Standard Practice for Preparing, Cleaning, and Evaluating Corrosion Test, ASTM International, 1-9 (2011).
18. NACE International, Laboratory Corrosion Testing of

Metals in Static Chemical Cleaning Solutions at Temperatures below 93°C (200°F), TM0193-2016-SG (2000).
19. A. Y. Issa, K. S. Rida, A. Q. Salam and A. A. Al-Amiery, Acetamidocoumarin as a based eco-friendly corrosion inhibitor, *International Journal of ChemTech Research*, , **9**, 39 (2016). https://sphinxsai.com/2016/ch_vol9_no11/abstracts/A(39-47)V9N11CT.pdf
20. M. Bairy, M. Pais, P. P. Kumari and S. A. Rao, Hydrazinecarbothioamide Derivative as an Effective Inhibitor for Corrosion Control: Electrochemical, Surface and Theoretical Studies, *Journal of Bio-and Tribo-Corrosion*, **8**, 1 (2022). Doi: https://doi.org/10.1007/s40735-021-00604-6
21. M. Galai, K. Dahmani, O. Kharbouch, M. Rbaa, N. Alzeqri, L. Guo, A. A. AlObaid, A. Hmada, N. Dkhireche, E. Ech-chihbi, M. Ouakki, M. Ebn Touhami and I. Warad, Surface analysis and interface properties of a newly synthesized quinoline-derivative corrosion inhibitor for mild steel in acid pickling bath: Mechanistic exploration through electrochemical, XPS, AFM, contact angle, SEM/EDS, and computational studies, *Journal of Physics and Chemistry of Solids*, **184**, 11169 (2024). Doi: https://doi.org/10.1016/j.jpcs.2023.111681
22. M. J. Frisch, G. W. Trucks, H. B. Schlegel, G. E. Scuseria, M. A. Robb, J. R. Cheeseman, J. A. Montgomery, Jr., T. Vreven, K. N. Kudin, J. C. Burant, J. M. Millam, S. S. Iyengar, J. Tomasi, V. Barone, B. Mennucci, M. Cossi, G. Scalmani, N. Rega, G.A. Petersson, H. Nakatsuji, M. Hada, M. Ehara, K. Toyota, R. Fukuda, J. Hasegawa, M. Ishida, T. Nakajima, Y. Honda, O. Kitao, H. Nakai, M. Klene, X. Li, J. E. Knox, H. P. Hratchian, J. B. Cross, V. Bakken, C. Adamo, J. Jaramillo, R. Gomperts, R. E. Stratmann, O. Yazyev, A. J. Austin, R. Cammi, C. Pomelli, J. W. Ochterski, P. Y. Ayala, K. Morokuma, G. A. Voth, P. Salvador, J. J. Dannenberg, V. G. Zakrzewski, S. Dapprich, A.D. Daniels, M. C. Strain, O. Farkas, D. K. Malick, A. D. Rabuck, K. Raghavachari, J. B. Foresman, J. V. Ortiz, Q. Cui, A.G. Baboul, S. Clifford, J. Cioslowski, B. B. Stefanov, G. Liu, A. Liashenko, P. Piskorz, I. Komaromi, R. L. Martin, D. J. Fox, T. Keith, M.A. AlLaham, C. Y. Peng, A. Nanayakkara, M. Challacombe, P. M. W. Gill, B. Johnson, W. Chen, M.W. Wong, C. Gonzalez and J. A. Pople, Cycloreversion of 4*H*-1,3-Thiazines and Selenazines Analogous: Theoretical Study by The Density Functional Theory (DFT) Method, *Journal of Materials Physics and Chemistry,* **6**, 23 (2018). https://www.sciepub.com/jmpc/abstract/9186
23. Gaussian 03, Revision B.05, Gaussian, Inc., Wallingford CT (2004).
24. T. Koopmans, Ordering of wave functions and eigenenergies to the individual electrons of an atom, Physica, **1**, 104 (in German) (1934). Doi: https://doi.org/10.1016/S0031-8914(34)90011-2
25. M. M. Solomon, H. Gerengi and S. A. Umoren, Carboxymethyl Cellulose/Silver Nanoparticles Composite: Synthesis, Characterization and Application as a Benign Corrosion Inhibitor for St37 Steel in 15% H_2SO_4 Medium, *ACS Applied Materials Interfaces*, **9**, 6376 (2017). Doi: https://doi.org/10.1021/acsami.6b14153
26. N. Khalil, Quantum chemical approach of corrosion inhibition, *Electrochimica Acta*, **48**, 2635 (2003). Doi: https://doi.org/10.1016/S0013-4686(03)00307-4
27. F. Zhang, Y. Tang, Z. Cao, W. Jing, Z. Wu and Y. Chen, Performance and theoretical study on corros inhibition of 2-(4-pyridyl)-benzimidazole for mild steel in hydrochloric acid, *Corrosion Science*, **61**, 1 (2012). Doi: https://doi.org/10.1016/j.corsci.2012.03.045
28. E. Ituen, O. Akaranta, A. James and S. Sun, Green and sustainable local biomaterials for oilfield chemicals Griffonia simplicifolia extract as steel corrosion inhibitor in hydrochloric acid, *Sustainnable Materials and Technology*, **11**, 12 (2017). Doi: https://doi.org/10.1016/j.susmat.2016.12.001
29. Z. Salarvand, M. Amirnasr, M. Talebian, K. Raeissi and M. Meghdadi, Enhanced corrosion resistance of mild steel in 1 M HCl solution by trace amount of 2-phenylbenzothiazole derivatives: Experimental, quantum chemical calculations and molecular dynamics (MD) simulation studies, *Corrosion Science*, **114**, 133 (2017). Doi: https://doi.org/10.1016/j.corsci.2016.11.002
30. S. O. Adejo and M. M. Ekwenchi, Proposing a new empirical adsorption isotherm known as Adejo-Ekwenchi isotherm, IOSR *J. Appl. Chem.*, **2014**, 6, 66-71.
31. I. D. Mall, V. C. Srivastava, N. K. Agrwal and I. M. Mishra, Adsorptive removal of malachite green dye from aqueous solution by bagasse fly ash and activated carbonkinetic study and equilibrium isotherm analysis, *Colloids and Surfaces A: Physicochemical and Engineering Aspects*, **264**, 17 (2005). Doi: https://doi.org/10.1016/j.colsurfa.2005.03.027
32. K. O. Sulaiman, A. T. Onawole, O. Faye, & D. T. Shuaib, Understanding the corrosion inhibition of mild steel by selected green compounds using chemical quantum based assessments and molecular dynamics simulations, *Journal of Molecular Liquids*, **279**, 342 (2019). Doi:

https://doi.org/10.1016/j.molliq.2019.01.136

33. S. L. Granese, B. M. Rosales, C. Oviedo, & J. O. Zerbino, The inhibition action of heterocyclic nitrogen organic compounds on Fe and steel in HCl media, *Corrosion. Science*, **33**, 1439 (1992). Doi: https://doi.org/10.1016/0010-938X(92)90182-3
34. W. Villamizar-Suarez, J. M. Malo, A. Martinez-Villafañe, & J. G. Cha-con-Nava, Evaluation of corrosion inhibitors performance using real-time monitoring methods, *Journal of Applied Electrochemistry*, **41**, 1269 (2011). Doi: https://doi.org/10.1007/s10800-011-0333-9
35. E. Berdimurodov, A. Kholikov, K. Akbarov, I.B. Obot and L. Guo, Thioglycoluril derivative as a new and effective corrosion inhibitor for low carbon steel in a 1 M HCl medium: Experimental and theoretical investigation, *Journal of Molecular Structure*, **1234**, 130165 (2021). Doi: https://doi.org/10.1016/j.molstruc.2021.130165
36. Q. Wang, L. Liu, Q. Zhang, X. Wu, H. Zheng, P. Gao, G. Zeng, Z. Yan, Y. Sun, Z. Li and X. Li, Insight into the anti–corrosion performance of Artemisia argyi leaves extract as eco–friendly corrosion inhibitor for carbon steel in HCl medium, *Sustainable Chemistry and Pharmacy*, **27**, 100710 (2022). Doi: https://doi.org/10.1016/j.scp.2022.100710
37. L. Huang, Q. Zhao, H.J. Li, J.Y. Wang, X.Y. Wang and Y.Ch. Wua, Investigation of adsorption and corrosion inhibition property of Hyperoside as a novel corrosion inhibitor for Q235 steel in HCl medium, *Journal of Molecular Liquids*, **364**, 120009 (2022). Doi: https://doi.org/10.1016/j.molliq.2022.120009
38. H. Lgaz, A. Chaouiki, M. Chafiq, R. Salghi, H. Tachallait, K. Bougrin, H.Y. Chi, C. Kwon and I.M. Chung, Evaluating the corrosion inhibition properties of novel 1,2,3-triazolyl nucleosides and their synergistic effect with iodide ions against mild steel corrosion in HCl: A combined experimental and computational exploration, *Journal of Molecular Liquids*, **338**, 116522 (2021). Doi: https://doi.org/10.1016/j.molliq.2021.116522
39. A. Farhadian, A. Rahimi, N. Safaei, A. Shaabani, M. Abdouss and A. Alavie, A theoretical and experimental study of castor oil-based inhibitor for corrosion inhibition of mild steel in acidic medium at elevated temperatures, *Corrosion Science*, **175**, 108871 (2020). Doi: https://doi.org/10.1016/j.corsci.2020.108871
40. X. Zheng, S. Zhang, W. Li, M. Gong and L. Yin, Experimental and theoretical studies of two imidazolium-based ionic liquids as inhibitors for mild steel in sulfuric acid solution, *Corrosion Science*, **95**, 168 (2015). Doi: https://doi.org/10.1016/j.corsci.2015.03.012
41. M. Rezaeivala, S. Karimi, K. Sayin and B. Tüzün, Experimental and theoretical investigation of corrosion inhibition effect of two piperazine-based ligands on carbon steel in acidic media, *Colloids and Surface, A: Physicochemical and Engineering Aspects*, **641**, 128538 (2022). Doi: https://doi.org/10.1016/j.colsurfa.2022.128538
42. A. S. Fouda, M. A. Ismail, A. S. Abousalem and G. Y. Elewady, Experimental and theoretical studies on corrosion inhibition of 4-amidinophenyl-2,2'-bifuran and its analogues in acidic media, *RSC Advances*, **7**, 46414 (2017). Doi: https://doi.org/10.1039/C7RA08092A
43. L.O. Olasunkanmi, I.B. Obot, M.M. Kabanda and E.E. Ebenso, Some quinoxalin-6-yl derivatives as corrosion inhibitors for mild steel in hydrochloric acid: Experimental and theoretical studies,*The Journal of Physical Chemistry C*, **119**, 16004 (2015). Doi: https://doi.org/10.1021/acs.jpcc.5b03285
44. P. Udhayakala, T. V. Rajendirin and S. Gunasekaran, Theoretical Evaluation of Corrosion Inhibition Performance of Some Triazole Derivatives, *Journal of Advanced Scientific Research*, **3**, 71 (2012). https://sciensage.info/index.php/JASR/article/view/101
45. H. Ma, S. Chen, Z. Liu and Y. Sun, Theoretical elucidation on the inhibition mechanism of pyridine-pyrazole compound: a Hartree Fock study, *Journal of Molecular Structure: THEOCHEM*, **774**, 19 (2006). Doi: https://doi.org/10.1016/j.theochem.2006.06.044
46. B. D. B. Tiu and R. C. Advincula, Polymeric Corrosion Inhibitors for the Oil and Gas Industry: Design Principles and Mechanism, *Reactive and Functional Polymers*, **95**, 25 (2015). Doi: https://doi.org/10.1016/j.reactfunctpolym.2015.08.006
47. M. Lagrenée, B. Mernari, M. Bouanis, M. Traisnel and F. Bentiss, Study of the mechanism and inhibiting efficiency of 3,5-bis(4-methylthiophenyl)-4H-1,2,4-triazole on mild steel corrosion in acidic media, *Corrosion Science*, **44**, 573 (2002). Doi: https://doi.org/0.1016/S0010-938X(01)00075-0
48. M. D. Plotnikova, A. D. Solovyev, A. B. Shein, A. N. Vasyanin and A. S. Sofronov, Corrosion inhibition of mild steel by triazole and thiadiazole derivatives in 5 M hydrochloric acid medium, *International Journal of Corrosion and Scale Inhibition,* **10**, 1336 (2021). Doi: https://doi.org/10.17675/2305-6894-2021-10-3-29
49. Sheetal, S. Sengupta, M. Singh, S. Thakur, B. Pani, P.

Banerjee, S. Kaya, and A. K. Singh, An insight about the interaction of Aryl Benzothiazoles with mild steel surface in aqueous HCl solution, *Journal of Molecular Liquids*, **354**, 118890 (2022). Doi: https://doi.org/10.1016/j.molliq.2022.118890

50. Q.-Q. Liao, Z.-W. Yue, Z.-W. Zhu, Y. Wang, Y. Zhang, G.-D. Zhou and Q. Zhou, Corrosion Inhibition Effect of Self-Assembled Monolayers of Ammonium Pyrrolidine Dithiocarbamate on Copper, *Acta Physico-Chimica Sinica*, **25**, 1655 (2009). Doi: https://doi.org/10.3866/PKU.WHXB20090811
51. A.A. Al-Amiery, Anti-corrosion performance of 2-isonicotinoyl-N-phenylhydrazinecarbothioamide for mild steel hydrochloric acid solution: Insights from experimental measurements and quantum chemical calculations, *Surface Review and Letters*, **28**, 2050058 (2021). Doi: https://doi.org/10.1142/S0218625X20500584
52. B. S. Mahdi, H. S. S. Aljibori, M. K. Abbass, W. K. Al-Azzawi, A. H. Kadhum, M. M. Hanoon, W. N. R.W Isahak, A. A. Al-Amiery and H. Sh. Majdi, Gravimetric analysis and quantum chemical assessment of 4-aminoantipyrine derivatives as corrosion inhibitors, *International Journal of Corrosion and Scale Inhibition*, **11**, 1191 (2022). Doi: https://doi.org/10.17675/2305-6894-2022-11-3-17